Search for gamma-ray emission from a galactic supernova with the anticoincidence system of SPI

M. Caixach, P. Jean, J. Isern, E. Bravo

Monthly Notices of the ROYAL ASTRONOMICAL SOCIETY

MNRAS **513,** 2814–2821 (2022) https://doi.org/10.1093/mnras/stac1089
Advance Access publication 2022 April 22

Search for gamma-ray emission from a galactic supernova with the anticoincidence system of SPI

M. Caixach [1,2]★ P. Jean,[3,4] J. Isern[1,2,5] and E. Bravo [6]

[1]*Institut de Ciències de l'Espai (ICE, CSIC), Campus UAB, C/ de Can Magrans s/n, E-08193 Cerdanyola del Vallès, Spain*
[2]*Institut d'Estudis Espacials de Catalunya (IEEC), C/ Gran Capità 2-4, E-08034 Barcelona, Spain*
[3]*Universiteé de Toulouse, UPS-OMP, IRAP, F-31028 Toulouse, France*
[4]*Institut de Recherche en Astrophysique et Planétologie, 9 Av colonel Roche, BP44346, F-31028 Toulouse Cedex 4, France*
[5]*Fabra Observatory, Royal Academy of Sciences and Arts of Barcelona (RACAB), La Rambla 115, E-08002 Barcelona, Spain*
[6]*E.T.S.A.V., Univ. Politècnica de Catalunya, c/Pere Serra 1-15, E-08173 Sant Cugat del Vallès, Spain*

Accepted 2022 April 12. Received 2022 April 6; in original form 2022 January 18

ABSTRACT

The detection of the very early gamma-emission of a Type Ia supernova (SNIa) could provide a deep insight on the explosion mechanism and nature of the progenitor. However, this has not been yet possible as a consequence of the expected low luminosity and the distance at which all the events have occurred up to now. An SNIa occurring in our Galaxy could provide a unique opportunity to perform such a measurement. The problem is that the optical flux would probably be so attenuated by interstellar extinction that it would prevent triggering the observations with gamma-spectrometers at the due time. In this paper, we analyse the possibility of using the anticoincidence system (ACS) of the spectrometer SPI on board of the *INTEGRAL* space observatory for detecting the early gamma-ray emission of an SNIa as a function of the explosion model and distance, as well as of pointing direction. Our results suggest that such detection is possible at about 6–12 d after the explosion, and at the same time, we can discard missing any hidden explosion during the lifetime of *INTEGRAL*.

Key words: supernovae: general – transients: supernovae – gamma-rays: stars.

1 INTRODUCTION

Type Ia supernovae (SNIa) are one of the most energetic explosion events in the universe, with luminosity magnitudes comparable to the ones from galaxies. These types of supernovae are identified by the lack of H lines and for having strong Si lines in the early spectra (Filippenko 1997). The optical light curve of SNIa peaks at about 20 d after the explosion and decreases by 3 mag after one month. They are the consequence of the thermonuclear explosion of a C/O white dwarf (WD) that accretes mass from a companion in a close binary (Hoyle & Fowler 1960). The discovery of several subtypes of SNIa these last years may be explained by SNIa possibly having more than one kind of progenitor scenarios and explosion mechanisms (Hillebrandt & Niemeyer 2000; Maoz, Mannucci & Nelemans 2014; Isern et al. 2021).

Even though the progenitor system and explosion mechanism of such events are not yet proved, one thing is known to be sure about SNIa: their optical luminosities are powered by the decay chain ^{56}Ni → ^{56}Co → ^{56}Fe. ^{56}Ni is synthesized during the rapid C/O burning and it fuels the explosion by the release of high-energy gamma-ray photons that heat the debris and power the optical and infrared light curves of the event (see Colgate & McKee 1969). The detection of gamma-ray lines from this decay can give clues about the kinematics and morphology of the explosion (Burrows & The 1990; Gomez-Gomar, Isern & Jean 1998; Jean et al. 1999; Milne et al. 2004; Isern, Bravo & Hirschmann 2008). The most prominent lines from ^{56}Ni decay are 158, 480, 750, and 812 keV, and from ^{56}Co decay are 847 and 1238 keV. They can be detected once the ejecta is thin enough in order for the gamma-ray photons to escape without getting thermalized. The decay of ^{56}Co has a mean lifetime of ∼111 d and its lines can be detected right after the maximum of the optical light curve and the following months. The intensity and broadening of the lines give information about the composition of the inner layers. On the other hand, the decay of ^{56}Ni has a mean lifetime of ∼8.8 d, which makes the detection of its gamma-ray lines somehow trickier, as for some explosion models, the opacity of the debris is too high for the photons to be able to escape without being absorbed. However, if there are radioactive elements in the outer layers, this gamma-ray emission can give the needed light to the study of the early stage of SNIa.

The closer SNIa ever detected in gamma-rays is SN2014J. It was discovered by Fossey et al. (2014). It was found in M82 at a distance of 3.5 Mpc. SPI instrument on board of *INTEGRAL* (INTErnational Gamma-RAy Laboratory) collected gamma-rays from day 16.3 to 164 after the explosion. The detection of ^{56}Ni and ^{56}Co lines of this nearby event allowed to prove the usefulness of gamma detection to diagnose the dynamics and composition of the ejecta (Churazov et al. 2014; Diehl et al. 2014; Isern et al. 2014; Churazov et al. 2015; Isern et al. 2016). The analysis of these observations not only confirmed the hypothesis that the light curve was powered by the disintegration of the ^{56}Ni radioactive chain but also allowed to compute in a direct way the total amount of ^{56}Ni synthesized during the event. Furthermore, they showed, unexpectedly, that ∼ 0.05 $M_\odot$ of ^{56}Ni was present in

★ E-mail: caixach@ice.cat

the outer layers, forming a non-spherical structure. The non-spherical structure was indicated by the display of redshifted and high intensity lines of ^{56}Ni in the early spectrum.

A Galactic supernova would be ideal for more detailed studies, especially if detected during the rising epoch of the light curve. The expected rate is estimated to be $1.4^{+1.4}_{-0.8}$ events per century (Adams et al. 2013) in the case of SNIa, and it is important to realize that the Galactic plane is transparent to gamma-rays for which reason events severely obscured by dust can be detected in gamma. Therefore, taking into account that *INTEGRAL* has been operating during ∼20 yr the probability that such an event has occurred during this period is not negligible.

The anticoincidence system (ACS) of SPI is used not only to reduce the background of SPI but also to monitor the sky for possible sources thanks to its large field of view and its spectroscopic capabilities (Vedrenne et al. 2003). Jean et al. (1999) proposed the use of the SPI-ACS to search for Galactic classical novae, Von Kienlin, Arend & Lichti (2001) to locate Gamma-ray bursts (GRBs), and Rodríguez-Gasén et al. (2014) to study solar flares. The scope of this paper is to study the ability of SPI-ACS to detect Galactic Type Ia supernovae as soon as possible (Wang, Fields & Lien 2019) and, in addition, to scrutinize the presence of its signature in the already recorded ACS data.

This paper is organized as follows: In Section 2,we present the supernova models used to simulate the detection by the ACS. Section 3 describes the ACS data used for this study. The simulation method and the results of the analyses to estimate the sensitivity of the ACS are presented in Section 4. Section 5 is dedicated to the search for SNIa signature in the existing SPI/ACS data. Finally, in Section 6, we present the discussion and conclusions.

2 SUPERNOVA MODELS

Two models of SNIa, DDTe and W7, have been used for testing the possibility of detection by ACS/SPI. The spectra as a function of time of these models were obtained with one-dimensional (1D) simulations as in Gomez-Gomar et al. (1998). These models were compared with those obtained from SN 2011fe and SN 2014J by the instruments on board of *INTEGRAL* (Isern et al. 2013, 2014). Both are compatible with the upper limits deduced for SN 2011fe, but the SN 2014J case demands further considerations since the early spectra presented some features that were better interpreted by introducing non-spherical structures.

The DDTe is a sub-luminous SNIa model. It describes a situation in which the burning front starts as a deflagration that turns out into a detonation when it reaches a critical density. As a result, the material is processed into Fe-group and into intermediate-mass elements. This model ejects 0.51 $M_\odot$ of ^{56}Ni with a kinetic energy of 1.09×10^{51} erg. The W7 model is a normal luminous SNIa model (Nomoto, Thielemann & Yokoi 1984). In this model, a flame ignited near the centre propagates subsonically, thus allowing the expansion of the star and leaving some unburnt material. The W7 model, in particular, is characterized by a small portion of unburnt C–O and a large mass of burnt intermediate-mass elements. This model ejects 0.56 $M_\odot$ of ^{56}Ni with a kinetic energy of 1.24×10^{51} erg. Fig. 1 displays the light curve of both models for SNIa at 8 kpc. They have been obtained by integrating the spectrum models from 6 to 3684 keV for an SNIa at 8 kpc.

Fig. 2 displays the gamma-ray spectra of both models in a logarithmic scale during the 9th day after the explosion. Even at such early stages, the 750 and 812 keV ^{56}Ni lines decay are visible, including several features from the ^{56}Co decay.

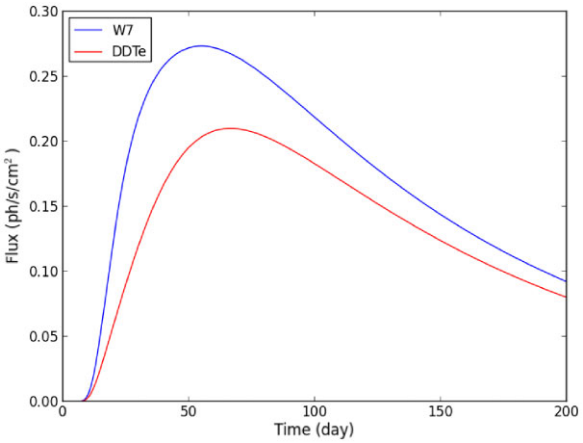

Figure 1. Gamma-ray flux variation for model W7 (blue) and DDTe (red) at a distance of 8 kpc from day 5th to day 200th after the explosion.

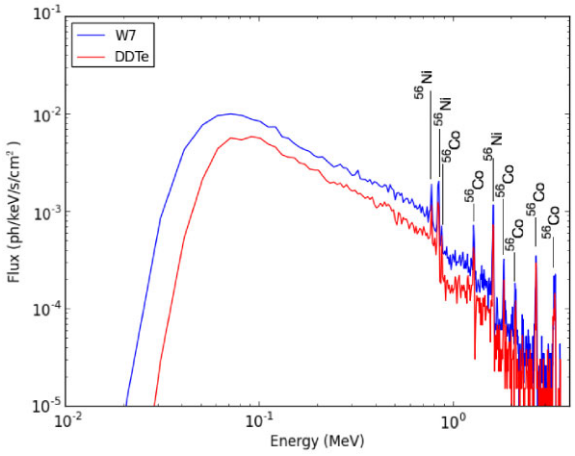

Figure 2. Gamma-ray spectra for day 9th of the models, W7 (blue) and DDTe (red) at 8 kpc. A label on top of each line is added to indicate if they are from ^{56}Ni or ^{56}Co decay.

The slow rising signal of the DDTe model as compared to that of W7 is a convenient property for exploring if the differences in luminosity have an impact on the detection sensitivity. In order to analyse the detection sensitivity as a function of SNIa distance, models were placed at distances in a range of 4–16 kpc. For each model, the output flux is provided with an energy resolution of 0.5 keV, in the interval 6–3684 keV. The spectra were calculated with a frequency of 1 d from days 5 to 200 after the explosion, although just the spectra derived for the first few days were used and interpolated, as the main goal is to study the detection of the rising signal as soon as possible. For further details about the models' data preparation, see Section 4.

3 THE ANTICOINCIDENCE SYSTEM (ACS) OF SPI

The ACS of SPI aims first to reduce the instrumental background in the germanium detectors due to charged particles and gamma-rays coming from outside the spectrometer's field of view. It is composed

of an active shield made with 91 scintillator blocks[1] in bismuth germanate (BGO) and a plastic scintillator, optically coupled to photomultiplier tubes (see Von Kienlin et al. 2001, for a detailed description of the SPI ACS). When a particle releases energy in a scintillator block, a veto signal is generated and transmitted to the on-board digital acquisition system. By this way, the active shield allows to remove events produced in coincidence by particles that deposit energy in the shield and in the germanium detectors. The ACS veto rate is recorded with a sampling period of 50 ms and is sensitive to photons releasing energy $\gtrsim 80$ keV in a scintillator block.

The ACS of SPI is also used to monitor astrophysical sources. For instance, its large detection area allows the detection of GRBs and it is part of the *INTEGRAL* burst alert system providing the GRB location in the sky by triangulations with other space-borne GRB monitors (Von Kienlin et al. 2001, 2003; Savchenko et al. 2017). A giant outburst from the soft gamma-ray repeater SGR 1806-20 was discovered in 2004 by the analysis of the ACS rate (Borkowski et al. 2004; Mereghetti et al. 2005). Rodríguez-Gasén et al. (2014) and Gros et al. (2004) explored the capabilities of the SPI ACS to study solar flares. Jean et al. (1999) proposed to use SPI ACS to search for the hard X-ray and gamma-ray emission from classical novae in our Galaxy (see also Siegert et al. 2018). For this purpose, they computed the effective area of the SPI ACS with GEANT 3 for energies ranging from 80 to 500 keV and a rough angular binning.

For the present study, we re-calculated the response of the SPI ACS with GEANT 4, using the same *INTEGRAL* mass model, for energies ranging from 80 keV to 3.5 MeV and with a binning of 10° for the zenithal and azimuthal angles (see Fig. 3). The mass model of *INTEGRAL* (see Fig. 4) was developed by Ferguson et al. (2003). It includes the SPI mass model developed by the SPI collaboration (see Sturner et al. 2003). For a given photon energy, the response was calculated assuming a point source at infinity (i.e. parallel beam) at a given angular position, by counting the number of events with energy deposit larger than the threshold of 80 keV. The effective area is equal to the number of triggering events divided by the number of simulated photons and multiplied by the exposed area, perpendicular to the parallel beam, in the simulation. The values of the effective area obtained in this way are close (within $\sim\pm30$ per cent) to the previous ones; e.g. $\sim 397\,\mathrm{cm}^2$ for $E > 100$ keV at a zenith angle of 100° and an azimuth angle of 0°, compared to the value of $340\,\mathrm{cm}^2$ close to the SGR 1806-20 position (see Mereghetti et al. 2005). They are also in agreement with the effective areas calculated by Rodríguez-Gasén et al. (2014) (e.g. differences are less than 5 per cent), who used the same *INTEGRAL* mass model to estimate the gamma-ray flux from some selected solar flares.

The ACS of SPI also provides the saturating event rate, defined as the rate of events released in the BGO blocks with energy $\gtrsim 150$ MeV. The ACS saturating event rate, unlike the ACS rate, is not affected by low energy particles from the radiation belt, from solar flares, or from gamma-ray sources that emit mainly in the low energy gamma-ray range (i.e. $E < 100$ MeV). Consequently, that makes it a good tracer for monitoring the cosmic ray intensity at the spacecraft level. When the spacecraft is not affected by these low-energy events, the temporal behaviour of the ACS saturating rate is concordant with the total ACS rate. Fig. 5 shows the average ACS rates and the average ACS saturating rates for some revolutions since the launch of *INTEGRAL*. In order to avoid the effects of radiation belts, the rates shown are the rates averaged over the first to the third quarter of each revolution. Fig. 5 shows that the total and saturating rates follow a linear relation, although the linear coefficients may slightly change due to slight changes of the high energy particle spectrum impinging the ACS. The saturating rate can therefore be used to trace the variation of the ACS rate without source contribution and be used as background model to our study (see Section 4.2).

[1]Only 89 blocks are active (see Savchenko, Neronov & Courvoisier 2012)

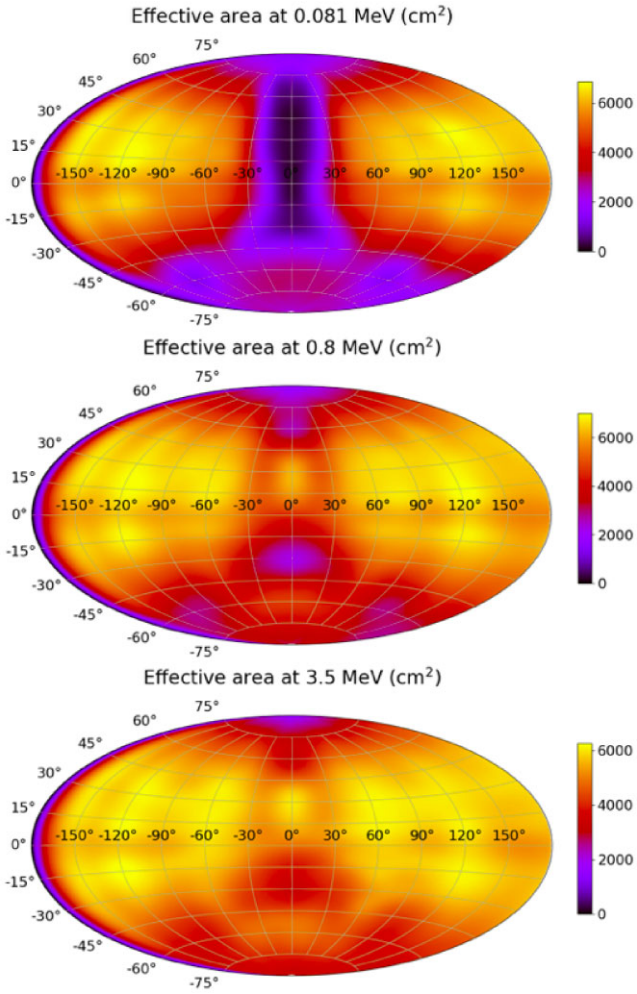

Figure 3. Effective area (cm^2) of SPI for energies of 0.081, 0.8, and 3.5 MeV for all pointing directions in the sky. The effective area is lower for regions where $z = 0°$ and the energies are low, and this is due to SPI being masked by IBIS.

4 SIMULATIONS AND ANALYSES

4.1 Simulated count rate

The count rate (CR), counts per second, from a source located at a zenithal and azimuthal angles θ and φ in the SPI frame at the instant t can be defined as:

$$R_{\mathrm{sn}}(t) = \sum_{E_i} F(E_i, t) \cdot S_{\mathrm{eff}}[E_i, \theta(t), \varphi(t)] \cdot \Delta E \qquad (1)$$

where $F(E_i, t)$ (counts $\mathrm{cm}^{-2}\,\mathrm{s}^{-1}\,\mathrm{keV}^{-1}$) is the flux for a given energy and time, $S_{\mathrm{eff}}[E_i, \theta(t), \varphi(t)]$ is the effective area (cm^2 – i.e. the response matrix) of the ACS and ΔE is the size of the energy bin (keV) of the spectrum. Overall it provides the rate in counts/s, R_{sn}, that would be produced by an SN model. Two SNIa models (see Section 2) have been simulated, the W7 model and a delayed

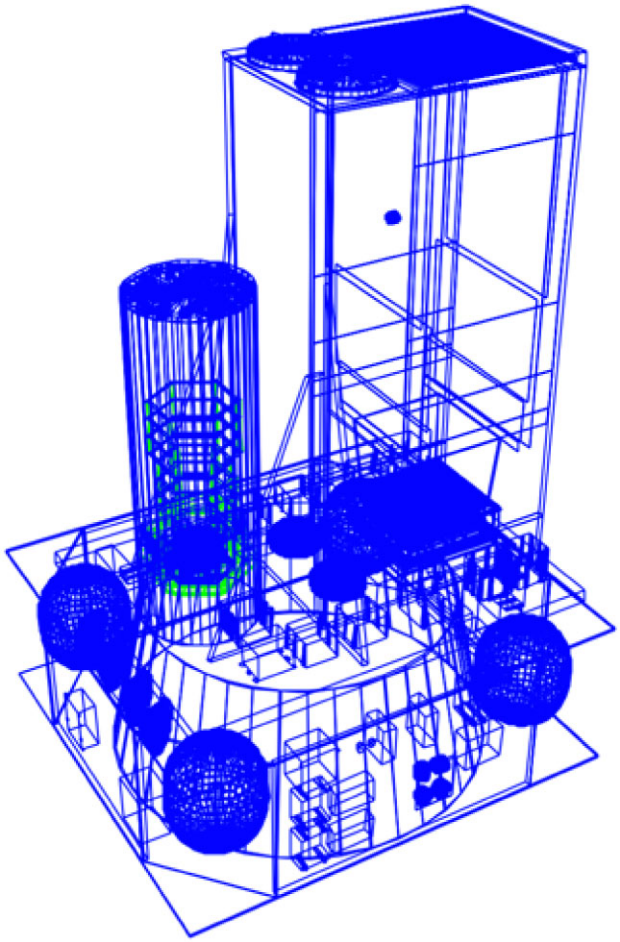

Figure 4. Mass model of *INTEGRAL* used to calculate the response of the ACS of SPI (in green) with GEANT 4 (see text).

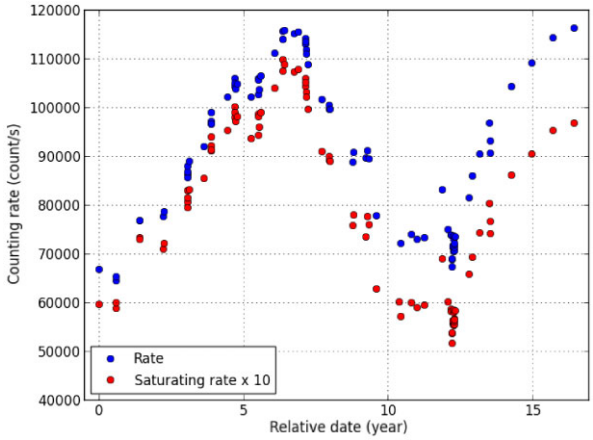

Figure 5. Total and saturating event rates of the ACS of SPI averaged for some revolutions since the launch of *INTEGRAL* (see text).

detonation model (DDTe), with an energy binning of 0.5 keV and a time binning of 80 s to provide enough resolution. Furthermore, the models have been scaled to Galactic distances of 4, 6, 8, 10, 12, 14, and 16 kpc.

The response matrix has been computed by Monte Carlo simulations (see Section 3). It gives the effective area for energies in the range of 81 keV to 3.5 MeV, with an azimuthal resolution of 20° and a zenithal resolution of 10°.

An interpolation of the response matrix is used to take into account the influence of the pointing variation during each revolution on the effective area for each energy event reaching the satellite. *INTEGRAL* provides for each revolution the right ascension (RA) and declination (Dec) of the x-axis of the instrument and the RA and Dec of the z-axis. For running the tests, we fix the RA and Dec of the simulated source and we take into account the angular evolution of the source with respect to the x- and z-axis of the instrument to obtain the local coordinates and, finally, the effective area.

INTEGRAL provides ACS data throughout the lifetime of the satellite for each orbital revolution. The ACS rate from a chosen revolution is added as a background to the SN model to make the simulated count rate realistic. We choose revolutions without strong background variations due to solar flares or early entrance in radiation belts. Each revolution has a duration between 2 and 3 d and the time of each revolution (and the SN model) is binned in intervals of 80 s. Before adding the ACS rate to the SN model rate, the first one needs to be converted from measured rate to true rate by taking into account the dead time δt of 0.6 μs (Savchenko et al. 2012):

$$R_{\rm bck} = \frac{R_{\rm m}}{R_{\rm m} \cdot \delta t - 1}, \tag{2}$$

where $R_{\rm bck}$ is the true background rate and $R_{\rm m}$ is the measured rate extracted from the data. The rate $R_{\rm sn}$ produced by the SNIa, computed with equation (1), is added to the true background rate to yield to the total rate $R_{\rm tot}$. The final simulated rate, $R_{\rm sim}$, is obtained with

$$R_{\rm sim} = \frac{R_{\rm tot}}{1 + R_{\rm tot} \cdot \delta t}, \tag{3}$$

to take into account the dead time of the ACS.

4.2 Detection of the supernova signal

Once the ACS rate produced by the supernova is simulated, we aim to study the sensitivity of the SPI ACS to detect the earliest gamma-ray signature of our SN models within a galactic distance. Two *methods* have been tested.

The first one consists of an 'ON/OFF'. It analyses a previous adjacent window (or interval) in the data, called the 'off' window, which represents a null hypothesis, and the subsequent window with the same size, the 'on' window, which represents an hypothetical source (Li & Ma 1983). A rising of significance is expected when the 'on' window has a rapid increase of flux compared to the previous 'off' window. This method, however, has been discarded as the significance of the detections is not high enough. Indeed, when that method is applied, the rate in the 'off' period contains the low signal from events produced in the ACS by the rising gamma-ray emission from the SNIa. The background rate is therefore overestimated. The contribution of the rising signal in the background rate reduces the significance of the detection.

The second method estimates the detection of the rising signal of the supernova by fitting the intensity of the supernova rate and the parameters of a background rate model to the SPI/ACS data. This method takes into account two assumptions. The first one considers that the background rate model ($r_{\rm bck}$) is a linear function of the ACS saturating ($R_{\rm sat}$) event rate:

$$r_{\rm bck} = \frac{R_{\rm sat} - c}{f}, \tag{4}$$

with c and f as free parameters. The saturating event rate (rate ACS saturating) is the rate of events with energy released in the

BGO blocks with energies $\gtrsim 150$ MeV (see Section 3). The second assumption is that the rate produced by the rising gamma-ray flux of the supernova can be described as the following power law:

$$r_{\rm sn} = I \cdot (t/5)^{\beta}, \tag{5}$$

where I is the intensity and t is the time of the model. Both are free parameters. The power-law model is justified by the shape of the gamma-ray light curves when the emission is rising (see Fig. 1). The slope of the power-law β is equal to 18.9 for the W7 model and 14 for the DDTe one. These two different values of the slope do not impact on the results very much.

With these two assumptions, we obtain a total model $r_{\rm mod} = r_{\rm bck} + r_{\rm sn}$, where $r_{\rm bck}$ is the background model [see equation (4)] and $r_{\rm sn}$ is the supernova signal model [see equation (5)]. The best-fitting parameters (I, c, and f) are the ones that minimize the chi square calculated as

$$\chi^2 = \sum \left(\frac{R_{\rm sim} - r_{\rm mod}(I, c, f)}{\sigma_{\rm acs}} \right)^2 + 10\,(f - f_0)^2 + \left(\frac{c}{2000} \right)^2, \tag{6}$$

where $R_{\rm sim}$ is the simulated ACS rate [see equation (3)] and $\sigma_{\rm acs}$ is the standard deviation of the model and the ACS data. The second and third terms in the sum are penalty functions that avoid wrong best-fitting values of the parameters f and c. Without those penalty functions, the minimization process could converge towards local chi square minimum yielding to abnormal values of the parameters of the background model, f and c. It sometimes occurs when the signal of the supernova is strong. The parameter f_0 in equation (6) is an estimated mean value of the factor that scales the ACS total rate with the ACS saturated rate (see Fig. 5 and Section 3). The factors 10 and 2000 in equation (6) were chosen to limit the variations of f and c on a reasonable range of values.

From these results, we can estimate the detection date. To do so, we first estimate the quality of the background model ($r_{\rm bck}$) by computing a residual (δ):

$$\delta = \frac{R_{\rm sim} - r_{\rm bck}}{\sigma_{\rm acs}}. \tag{7}$$

Then, this residual is smoothed to avoid a false detection due to a single short time scale spike in the data.

We consider that the supernova signal is detected when the following conditions are satisfied: (1) $t_{\rm acs} > t_{\rm start} + 0.5$ d; (2) $\delta > 3$. Where $t_{\rm acs}$ is the time of the data, the sigma level is set to 3, and $t_{\rm start}$ is the date at which the ACS data starts to be recorded at the beginning of an orbital revolution of *INTEGRAL*. The addition of half a day in the first condition aims to remove significant count rate excess induced by high energy particles when *INTEGRAL* goes out of the radiation belts, after its perigee.

This procedure is done to test the DDTe SN model and the W7 SN model over 275 revolutions. These revolutions have been taken along the lifetime of *INTEGRAL* to find the earliest time of detection. Each of them has the following available data: ACS rate, ACS saturating rate, rate time, RA and Dec of the *INTEGRAL X*-axis, RA and Dec of the *INTEGRAL Z*-axis. The ACS rate is used as simulated background to the models, as mentioned in Section 4.1. The ACS saturating event rate is used on this analysis to estimate the background ACS rate and detect the supernova signal, as mentioned previously in this section. Each revolution has a length of 2–3 d that we fixed to ≈2 d as we cut the initial hours of data because most of them still contain some noise from the radiation belt phase.[2] A same length of the supernova model is cut in order to compute the simulated count rate. The initial time of the computed count rate equals to a time ranging from day 4th to 6th of the SNIa model, for earlier days the flux's model is not high enough to make a contribution to the ACS rate. This initial time, from 4th to 6th, is chosen randomly to give more realistic circumstances to the analysis.

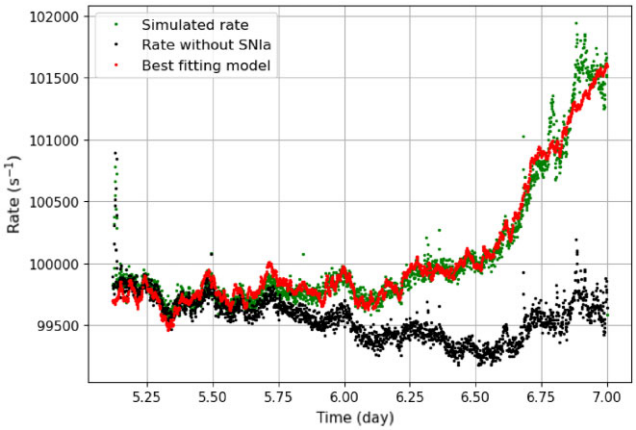

Figure 6. Display of the SN model rate with revolution number 1752 added as background in green. The background rate, without the SN signal, is shown in black. The best-fitting model to the SN with background rate is shown in red. For this example, the rising of the SN rate is appreciated and allows the detection time to be at 6.73 d.

When the count rate with a length of 2 d is analysed, two things may happen: a supernova signal detection is found or not. If a detection is found in the count rate then the revolution number, the time detection and its significance are saved. In case it is not, we proceed to analyse the consecutive 2 d of the computed count rate, which would account for the two following days of the SNIa model, using the subsequent revolution as its background. This procedure is repeated until a detection is found or until we reach an initial time of the count rate higher than the 10th of the SNIa model. When this point is reached, we start the process again with an initial count rate time ranging from 4th to 6th but with a different revolution as background and so on. An example output of this method is shown in Fig. 6, where the count rate is computed using the DDTe model with revolution number 1752. The computed discovery date is at 6.73 d with $\approx 67\sigma$, which is coherent if we make a visual evaluation of the count rate data.

In some cases, due to high background or too many changes in pointing direction in the same revolution, the rising of the SN model goes undetected, but on the following revolution, as the SN model flux is higher with time, the flux is too high to find a good fit. In these cases, an inspection of the data makes clear that there is a high rising signal and the satellite would recognize it as such. We want to count these cases as late detections, so a condition is created whereby, if the maximum of the SNIa signal is larger than 8.5 per cent of the mean ACS rate, the detection time is saved even if the fit is not good enough.

The analysis of the count rate has been performed for each of the models (DDTe and W7) for distances of 4, 6, 8, 10, 12, 14, and 16 kpc. For each distance and model, several pointing directions have been tested to reproduce different galactic areas backgrounds and to check the variability of the detection on different positions in the Galaxy.

[2]SPI is switched off between revolutions

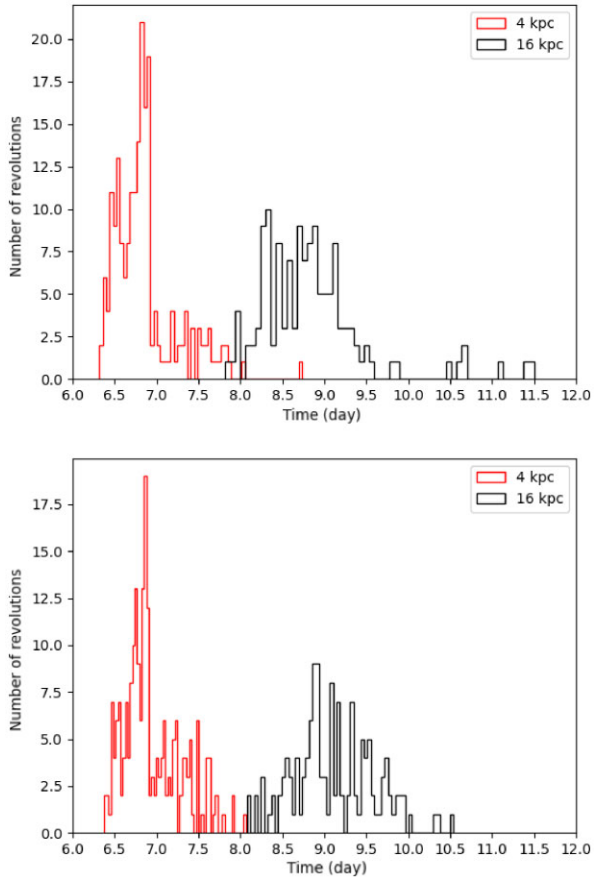

Figure 7. Top panel shows the distribution of the discovery dates for the W7 model at $l = 0^\circ$ and $b = 0^\circ$ for distances of 4 kpc (red) and 16 kpc (black). Bottom panel displays the same for the DDTe model.

The pointing directions, in galactic coordinates of longitude (l) and latitude (b), are $l = 0$, 45, 90, and 180° for $b = 0^\circ$. All the positions have the same value of latitude of $b = 0^\circ$. The reason for this fixed latitude is that the location for these events in our Galaxy would be in regions of old population stars, which are in the old disc and in a spheroid centred to the Galactic Centre. Therefore, they would likely occur at $\pm 15^\circ$ from the galactic plane. As seen in Fig. 3, the response of the ACS does not change significantly with the direction of the source (except for low energies). Hence, simplifying the latitude to $b = 0^\circ$ is good enough for our study.

4.3 Results

Following the methodology explained in Section 4.2, the time detection for the W7 and DDTe models placed at distances of 4, 6, 8, 10, 12, 14, and 16 kpc and at positions $l = 0$, 45, 90, and 180° with $b = 0^\circ$ has been computed. An example of two different distances, 4 and 16 kpc, and $l, b = 0^\circ$ is shown for models W7 and DDTe in Fig. 7, top and bottom panels, respectively. For both models, the number of detections for higher distances is lower due to the lower flux.

The mean value of the distribution is computed and shown for all distances and pointing directions in Fig. 8 for the W7 model and Fig. 9 for the DDT model. The time of the early signal detection for each distance is coherent with the flux $\propto$ distance^{-2} relation, as for further distances the detections are later due to lower flux. The W7 model has a slightly earlier detection for each case because of its faster rise compared to the DDTe one. The position of the source

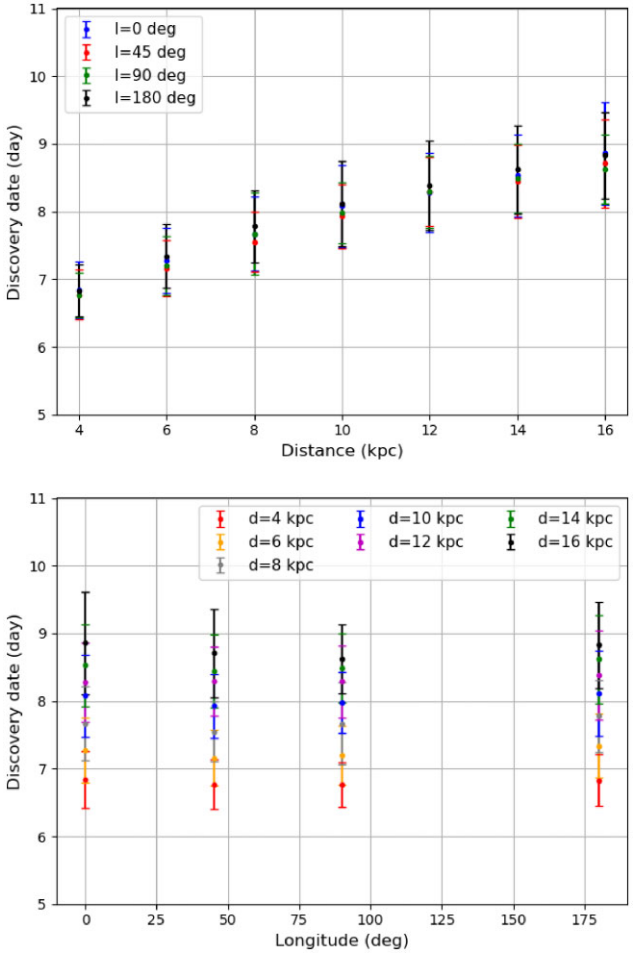

Figure 8. Mean discovery dates versus distance for model W7 (top panel) and longitude (bottom panel).

is not relevant for the early detection of the model, as it does not change for each longitude tested, see bottom panels of Figs 8 and 9. These results are due to the fact that *INTEGRAL* observatory has been pointing in various directions during the ∼15 yr of observation and that the equivalent field of view of the ACS/SPI is very large, so the position of an SNIa in the sky does not show any effect.

5 SEARCH OF SNIA SIGNATURE IN THE SPI/ACS DATA

We performed a systematic search for an SNIa signature in the ACS rate with the data available at the date of the analysis: 1868 revolutions from revolution 26 to revolution 2063. The analyses were made for each revolution using ACS data rebinned with a sampling period of 18 s. The detection of an SNIa signature is triggered when the smoothed residuals[3] obtained after subtraction of the background model (see section 4.2), are larger than 5σ up to the end of the analysed revolution. This criterion, which was chosen for its simplicity, allows the detection of a flux rising with a long timescale as to the one expected from an SNIa (e.g. see Fig. 6). A first analysis of all data yielded to a lot of detection due to background

[3]The residuals were smoothed with a hanning window of 1.5 h to reduce the number of detections due to GRBs and false detections due to statistical fluctuations.

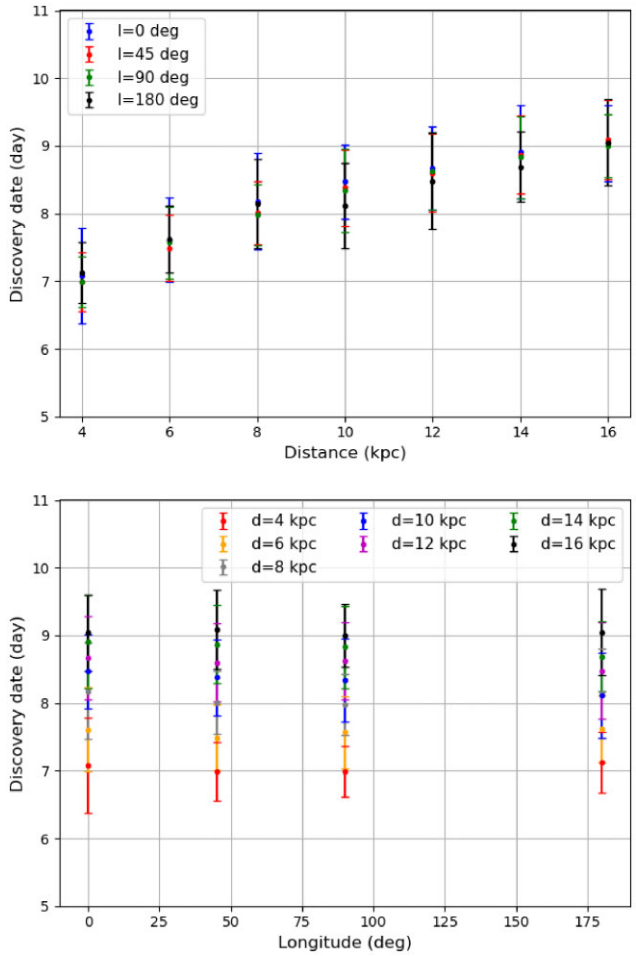

Figure 9. Mean discovery dates versus distance for model DDTe (top panel) and longitude (bottom panel).

variations, which spans up to the end of a revolution, that were not well modelled with the ACS saturating event rate. Those background variations are due to low energy particles of the radiation belt or from solar events. The signature of such particles is clearly seen in the data of the *INTEGRAL* Radiation Environment Monitor (IREM), which measures the flux of particles with energy >0.5 MeV for electron and 10 MeV for proton (Hajdas et al. 2003). The counter TC3 of the IREM reproduces well the variations of ACS rate produced by low energy charged particles of radiation belts. In order to reduce the number of detections due to low energy particles, we added the rate of the TC3 counter in the background model for this specific analysis.

With such a detection method, we counted 58 revolutions with SNIa signature. However, all of them are detected at dates larger than ∼2.2 d after the beginning of the revolution. These excesses are explained by an imperfect modelling of the enhancement of the rate produced by low energy particles impinging on the scintillators of the ACS when *INTEGRAL* enters into the radiation belt at the end of its orbital revolutions (e.g. see Fig. 10).

6 CONCLUSIONS

This study demonstrates the capability of the ACS/SPI to detect a galactic supernova during its early stages. Two theoretical SNIa models with different luminosities rising times, W7 and DDTe, have been used in order to evaluate the influence on the time of the detection. For such a purpose, we have developed a method to detect the signature of the rising flux emitted by a supernova and to derive a detection date as quickly as possible. Using simulations of the count rate produced by the source models and the measured background ACS rates of 275 orbital revolutions of *INTEGRAL*, we have found that our method allows to discover a galactic SN as soon as 6 d up to 12 d after explosion, depending on the distance and model.

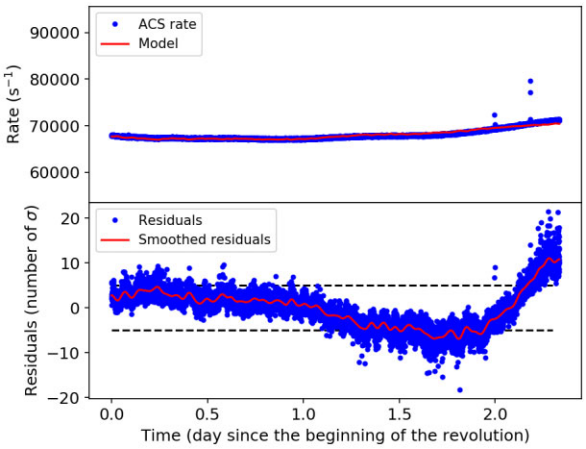

Figure 10. Example of measured and modelled ACS rates (top) and the residuals (bottom) for the revolution 1342. The imperfect modelling of the ACS rate at the end of the revolution, when *INTEGRAL* enters into radiation belts, produces a smoothed residual excess larger than 5σ.

The simulated sources have been placed at several distances (from 4 to 16 kpc), several galactic longitudes, and zero latitude. The discovery date increases with the distance, as the flux of the modelled sources is smaller. This result follows the distance flux relationship. On the other hand, the galactic longitude of the source has no influence on the discovery date, which is logical taking into account the large field of view of the ACS/SPI.

As the discovery date depends on the flux, we have found there is a slightly different range of discovery dates for the two models. The DDTe model is a sub-luminous SN Ia model and the W7 is a normal luminous one. The lower luminosity of the DDTe resulted in a detection range of approximately half-day later than the W7. Using our detection method, we have analysed all the available ACS/SPI data from the beginning of the *INTEGRAL* mission to now and we have not found any signature of a galactic SNIa, suggesting no event has been missed.

This method is not able to provide a position of a source but it can provide an early alert to activate others in orbit or ground-based observatories to quickly browse the sky in search for it. In any case, the collected data would provide very important information about the early development of the supernova outburst, no matter if the event is detectable in any other energy range. *INTEGRAL* is in its last stages of life and the results obtained here suggest that future missions should consider the possibility of using the ACS as an all-sky detector by improving its sensitivity, as much as possible. The new space telescope COSI,[4] which is expected to launch in 2026, will observe the gamma-ray sky in the 200–5 MeV range (Tomsick et al. 2022). It will be equipped of a compact Compton telescope made with germanium detectors and of an ACS made with BGO

[4]see website: https://www.nasa.gov/press-release/nasa-selects-gamma-ray-telescope-to-chart-milky-way-evolution

scintillators as for SPI. With its large field of view (∼25 per cent of the sky) and its pointing strategy, COSI will monitor the entire sky within a day. Both the Compton telescope and the ACS will be sensitive to the gamma-ray emission of a galactic SNIa.

ACKNOWLEDGEMENTS

The authors thank the anonymous referee for helpful comments. We acknowledge support from the Spanish Ministry of Science and Innovation and – FEDER UE (MCI-AEI-FEDER,UE) through grants PID2019-108709GB-I00 (MC,JI) and PGC2018-095317-B-C21 (EB), by grant 2014 SGR 1458 and CERCA Programme of the Generalitat de Catalunya (MC,JI), and by the programme Unidad de Excelencia María de Maeztu CEX2020-001058-M (MC,JI).

DATA AVAILABILITY

The SPI data used for this study are public data available in the ISDC website: http://www.isdc.unige.ch/integral/archive#DataRelease.

REFERENCES

Adams S. M., Kochanek C. S., Beacom J. F., Vagins M. R., Stanek K. Z., 2013, ApJ, 778, 164
Borkowski J., Gotz D., Mereghetti S., Mowlavi N., Shaw S., Turler M., 2004, GCN Circ. , 2920, 1
Burrows A., The L.-S., 1990, ApJ, 360, 626
Churazov E. et al., 2014, Nature, 512, 406
Churazov E. et al., 2015, ApJ, 812, 62
Colgate S. A., McKee C., 1969, ApJ, 157, 623
Diehl R. et al., 2014, Science, 345, 1162
Ferguson C. et al., 2003, A&A, 411, L19
Filippenko A. V., 1997, ARA&A, 35, 309
Fossey S. J., Cooke B., Pollack G., Wilde M., Wright T., 2014, Cent. Bur. Electron. Telegrams, 3792, 1
Gomez-Gomar J., Isern J., Jean P., 1998, MNRAS, 295, 1
Gros M. et al., 2004, in Schoenfelder V., Lichti G., Winkler C., eds, Proc. 5th INTEGRAL Workshop "The INTEGRAL Universe" Vol. 552. ESA Special Publication, Munich, p. 669
Hajdas W., Bühler P., Eggel C., Favre P., Mchedlishvili A., Zehnder A., 2003, A&A, 411, L43
Hillebrandt W., Niemeyer J. C., 2000, ARA&A, 38, 191
Hoyle F., Fowler W. A., 1960, ApJ, 132, 565
Isern J. et al., 2013, A&A, 552, A97
Isern J. et al., 2014, Astron. Telegram, 6099, 1
Isern J. et al., 2016, A&A, 588, A67
Isern J., Bravo E., Hirschmann A., 2008, New Astron. Rev., 52, 377
Isern J., Hernanz M., Bravo E., Grebenev S., Jean P., Renaud M., Siegert T., Vink J., 2021, New Astron. Rev., 92, 101606
Jean P. et al., 1999, Astrophys. Lett. Commun., 38, 421
Li T. P., Ma Y. Q., 1983, ApJ, 272, 317
Maoz D., Mannucci F., Nelemans G., 2014, ARA&A, 52, 107
Mereghetti S., Götz D., von Kienlin A., Rau A., Lichti G., Weidenspointner G., Jean P., 2005, ApJ, 624, L105
Milne P. A. et al., 2004, ApJ, 613, 1101
Nomoto K., Thielemann F. K., Yokoi K., 1984, ApJ, 286, 644
Rodríguez-Gasén R., Kiener J., Tatischeff V., Vilmer N., Hamadache C., Klein K. L., 2014, Sol. Phys., 289, 1625
Savchenko V. et al., 2017, A&A, 603, A46
Savchenko V., Neronov A., Courvoisier T. J. L., 2012, A&A, 541, A122
Siegert T. et al., 2018, A&A, 615, A107
Sturner S. J. et al., 2003, A&A, 411, L81
Tomsick J. A. et al., 2022, Proc. of the 37th International Cosmic Ray Conference held in Berlin. Online at, link, id.652.
Vedrenne G. et al., 2003, A&A, 411, L63
Von Kienlin A. et al., 2003, A&A, 411, L299
Von Kienlin A., Arend N., Lichti G. G., 2001, in Costa E., Frontera F., Hjorth J., eds, Proc. Int. workshop held in Rome, Gamma-ray Bursts in the Afterglow Era. Springer, Berlin, Heidelberg, p. 427
Wang X., Fields B. D., Lien A. Y., 2019, MNRAS, 486, 2910

This paper has been typeset from a TEX/LATEX file prepared by the author.